The International Journal of Advanced Manufacturing Technology
https://doi.org/10.1007/s00170-026-18334-9

ORIGINAL ARTICLE

Investigation on the mass finishing of 17-4PH steel produced via binder jetting for orthopedic surgical applications

Matteo Pozzi[1,2] · Andrea Lucchini Huspek[1] · Marco Mariani[3] · Sara Candidori[3] · Serena Graziosi[3] · Nora Lecis[3] · Silvia Franz[1] · Massimiliano Bestetti[1]

Received: 12 December 2025 / Accepted: 12 May 2026

Abstract
Binder Jetting is an innovative Additive Manufacturing process that was employed to produce 17-4PH steel components for orthopedic surgery applications, starting from pre-alloyed powders. Poor surface finishing of as-printed components often requires post-processing to comply with biomedical requirements. Mass finishing is a widely applied technology to lower roughness by means of mechanical abrasion. This study optimized a centrifugal disk machine mass finishing process for 17-4PH components produced by Binder Jetting. Surface printing orientation, abrasive paste composition, and precipitation hardening thermal treatment effects were investigated. Sample morphology was characterized by optical and scanning electron microscopy, roughness was measured by contact and confocal profilometry, material removal rate was estimated by mass loss measurements, and surface chemical composition was investigated by energy-dispersive X-ray spectroscopy. SiC, Al_2O_3, and SiO_2 containing abrasive pastes effectively reduced roughness across all printing orientations. Abrasive smoothening effectiveness was correlated with the material removal rate. SiC-based paste resulted in the highest roughness reduction, reaching an average Ra of 0.62 ± 0.25 µm after 4 h of treatment. Traces of mass finishing abrasive pastes were observed on the polished surfaces, not precluding biomedical compatibility for orthopedic surgical applications. Upon precipitation hardening treatment, Vickers hardness increased by 42%. As a consequence, the material removal rate and roughness reduction were slowed down. Experimental results indicated that performing the mass finishing process before thermal aging allows roughness requirements to be met in a shorter time.

Highlights
- Mass finishing in a centrifugal machine was employed to lower surface roughness on 17-4PH components produced via Binder Jetting.
- The effect of different abrasive pastes and process duration was systematically investigated, as well as the influence of the printing orientation.
- An average Ra of 0.62 ± 0.25 µm was obtained after 4 h of treatment with SiC abrasive paste on as-built 17–4 H samples.
- Mass finishing can be integrated into the production workflow of BJT-manufactured surgical instruments before H900 thermal aging.

Keywords Binder jetting · Mass finishing · Additive manufacturing · Surgical instruments

1 Introduction

Binder Jetting (BJT) is an Additive Manufacturing (AM) process based on the selective deposition of a ligand, usually an organic binder, on a powder bed through a layer-by-layer procedure. The printing process allows for producing a green component upon curing the whole powder bed at low temperatures. After a de-powdering step, the green body is debinded and sintered to the degree of densification desired. The BJT of ceramic [1] and metallic components is rapidly growing, especially for 17-4PH [2] and 316 l stainless steels [3–5], due to the availability of

Extended author information available on the last page of the article

Published online: 28 May 2026

spherical powders with controlled size distributions that allow optimal flowability and packing in the printing process. In particular, Salaheldin et al. investigated the effects of solution annealing and ageing treatments on the microstructure and mechanical properties of 17-4PH steel produced by BJT [2].

17-4PH is a high-strength, precipitation-hardening alloy whose mechanical performance is controlled by the formation of copper precipitates in a martensitic matrix upon solution annealing and thermal aging. The possibility of obtaining high hardness and yield strength combined with ductility is attractive for a series of applications in the biomedical industry. Several orthopedic surgical instruments, such as femoral broaches or bone-cutting guides, are made of 17-4PH stainless steel hardened by means of H900 or H1150 thermal treatments to achieve the mechanical properties required for preparing implant sites by bone reshaping, cutting, and drilling.

Beyond mechanical performance, however, surgical instruments must also satisfy stringent surface quality requirements to ensure proper functionality and biocompatibility during clinical use. A well-recognized limitation of AM processes is the relatively high surface roughness of as-built components [1, 2], which cannot be directly reconciled with biomedical surface standards. From a clinical perspective, surface roughness plays a critical role in determining the performance and safety of metallic surgical instruments: excessive roughness has been associated with increased bacterial adhesion [6], impaired cleanability [7], localized corrosion susceptibility, and early fatigue crack initiation [8, 9], all of which are particularly relevant for orthopedic tools subjected to cyclic mechanical loads and repeated sterilization [10, 11]. Consequently, average roughness values below approximately 1 µm are generally targeted for stainless steel surgical instruments to facilitate cleaning and minimize tissue trauma during transient contact with bone and soft tissues [7]. In contrast, BJT typically produces surfaces with Ra values in the range of 5–10 µm or higher [12–14], depending on build orientation, powder characteristics, and sintering conditions [15, 16], thereby substantially exceeding these functional thresholds. This discrepancy underscores the necessity of effective post-processing strategies to enable the clinical translation of BJT-manufactured orthopedic components. Among the available approaches, mass finishing represents an attractive industrial solution due to its scalability, batch processing capability, and potential to achieve significant roughness reduction within practical production times.

Thanks to its versatility and the possibility to treat many components simultaneously, mass finishing emerges as a valid solution to face AM components' surface quality [10, 17, 18]. Mass finishing processes are carried out in vibrating or rotating tanks, where components to be polished are loaded together with abrasive media, water and, possibly, chemical compounds [19, 20]: the mechanical abrasion of media on components surface provides for roughness reduction [20–22], edge deburring [23], and surface brightening [24–26]. Several applications of mass finishing processes for components produced by AM with Laser Beam Powder Bed Fusion (PBF-LB) technology are reported. The main finishing technologies frequently applied for AM parts include barrel finishing [27–29], vibro-finishing [8, 30, 31], and centrifugal disk finishing [32–34]. Processes last from 30 to 240 min for centrifugal disk machines [32, 33] up to 12–96 h for vibro-finishing [30, 35] and barrel finishing [29, 36]. They are usually carried out in wet conditions with ceramic or plastic abrasive media, whose shape and dimensions are tuned according to the sample geometry [17]. Multi-step processes are often needed to smooth surfaces with high initial roughness [35, 37, 38]. Mass finishing is currently widely applied in the biomedical industry to deburr and smooth components after mechanical machining [20, 39]. For these reasons, it is considered a suitable technology to improve surface quality also of AM metallic components for biomedical applications [31, 40].

Post-processing, other than mass finishing, for BJT components is reported to be beneficial in reducing roughness [5, 10, 41], improving corrosion resistance [12] and tribological properties [14]. Also, the fatigue behavior of BJT components can be influenced by surface finishing processes, since fatigue crack initiation is strongly affected by the roughness and porosity of the outermost printed layer [10, 33]. Despite the large number of post-processing solutions proposed for PBF-LB technology, the literature still lacks studies focused on the mass finishing of components produced by BJT. PBF-LB produces more compact specimens whose roughness arises from phenomena occurring in and close to the melt pool generated upon laser irradiation: surfaces are usually characterized by spatters, ballings, and partially melted powders. BJT specimens present the structure of sintered materials, and their roughness is the result of alternating protrusions and pores. As a consequence, dedicated post-processing processes have to be studied. In recent years, BJT has attracted conspicuous attention in the AM industry, mainly due to its high productivity and possibility of integration within the powder metallurgy industry [42]. It is therefore necessary to develop surface finishing processes suited to the demands of this emerging production technology. This aims to support the entire component production chain which does not end with the printing but

rather with surface post-processing. Mass finishing processes, being easily scalable and guaranteeing high productivity as well, appear to be an optimal process coupled with metal BJT.

The present work systematically investigates single-step mass finishing processes for 17-4PH components produced via BJT for orthopedic surgery instruments, highlighting their advantages and limitations. It targets to optimize a mass finishing process to be integrated into an orthopedic instrument production cycle, analyzing the surface features of polished components before and after the precipitation hardening (H900) heat treatment. For this purpose, the effect of different abrasive pastes and surface orientations on components' roughness and morphologies was considered. The overall aim is to assess the advantages and disadvantages of finishing the as-sintered components rather than heat-treated ones, focusing on the obtained final roughness and processing time.

2 Materials and methods

2.1 Sample BJT printing and heat treatment

A pre-alloyed stainless steel 17-4PH (AISI 630) powder was employed in the printing process. The feedstock was obtained through gas atomization to grant high sphericity and, thus, optimal packing within the powder bed. The declared particle size distribution featured a $D_{10}=10$ µm, $D_{50}=25$ µm, and $D_{90}=50$ µm; hence, a layer thickness of 75 µm was selected as the printing parameter. The specimens were manufactured by a Desktop Metal Shop System 3D printer (Aidro S.r.l., Milano, Italy). The coupons were manufactured in three primary orientations (Horizontal, Vertical, and Oblique in the following referred to as "H", "V" and "O" respectively) as illustrated in Fig. 1. To account for the inherent anisotropy of the BJT process, the upskin and downskin surfaces were distinguished for non-vertical

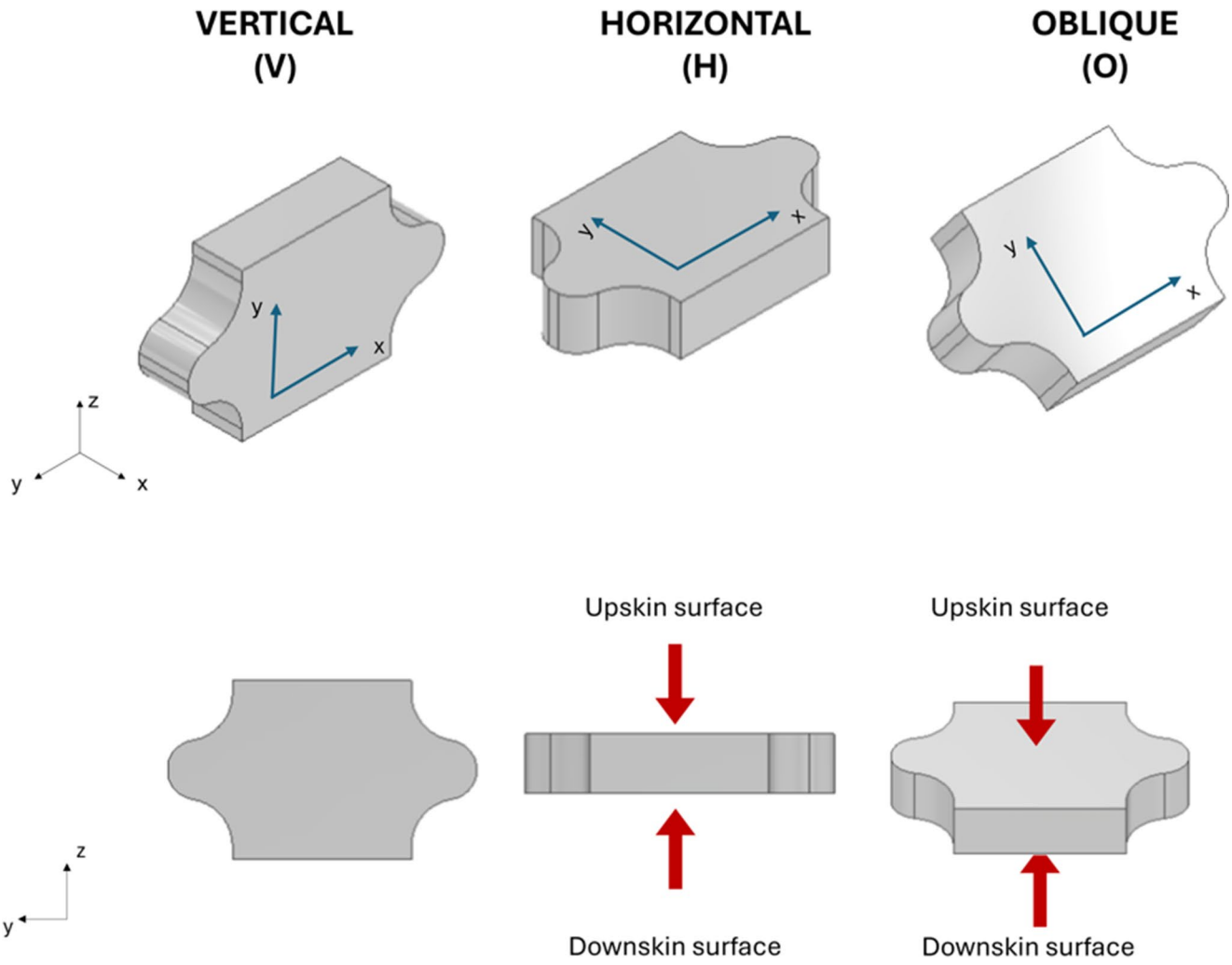

Fig. 1 Layout and orientation of the BJT-produced coupons within the build volume. The top portion of the figure provides an isometric view of the specimens, while the bottom panel presents the front view. For the horizontal and oblique coupons, the upskin (top-facing) and downskin (bottom-facing) surfaces are identified. The coordinate axes X and Y used for the subsequent analysis are indicated for each orientation

specimens. Furthermore, the surface topography analysis was conducted along the local X and Y axes indicated in Fig. 1, allowing for a standardized comparison across all build configurations. The components were cured in air at low temperature (<200 °C) to obtain consolidated green bodies and separated from the excess powder by manual brushing and air blowing.

The samples were then debinded and sintered in a multistep cycle performed in a slightly reducing atmosphere (97% Ar, 3% H_2) up to a maximum temperature of 1310 °C (hereinafter *as-sintered* samples). A set of samples, comprehending three samples printed in the three considered printing orientations (V, H, O), was thermally treated after the sintering to induce the precipitation of copper in the material and, as a consequence, improve the mechanical properties of the alloy. The components underwent a solution annealing treatment at 1050 °C for 1 h, followed by aging according to the H900 treatment at 480 °C for 1 h and then quenching (hereinafter labelled as the *thermally treated* samples). The thermal treatments were performed in a low vacuum (10^{-1} mbar) furnace (HT- S1 LPC, HTS Vacuum Furnaces), and the rapid cooling was obtained by flowing nitrogen to prevent oxidation. The Vickers microhardness was measured before and after the thermal treatment according to the ASTM A564-A564M-19 A standard [43], using a Future-Tech FM-810 indenter with a load of 300 gf applied for 15 s.

2.2 Surface finishing

Mass finishing tests were carried out in a centrifugal High Energy Disk Machine FKS 02 (Rösler Italiana S.r.l., Concorezzo, Italy), running at 250 rpm, loaded with 11 kg of RCP 04/10 ZS cylindrical media (Rösler Italiana S.r.l., Concorezzo, Italy), 300 ml of abrasive paste (Rösler Italiana S.r.l., Concorezzo, Italy), and 6 l of tap water. The selection of process parameters such as the rotational speed, the volume of media and water, and the water-to-abrasive paste ratio was done based on supplier experience. The rotation speed tends to increase the abrasive effect since it increases the speed at which the media and the pieces impact each other, for this reason the maximum allowed speed was set. The volume of the media was such that two-thirds of the available volume were filled; while the volume of water was such that it completely covered the mass of media during the rotational motion. Machine parameter optimization was beyond the scope of this work. Three different abrasive pastes were tested whose commercial names are RSP (Rösler Special Paste) 587, RPP (Rösler Polishing Paste) 520, and RPP 579: their main abrasive components are SiC, Al_2O_3, and SiO_2, respectively. Pastes presented similar features regarding the number of abrasive particles (≥50 wt%) and their granulometric distribution. After each hour of the test, samples were ultrasonically washed in deionized water and dried before characterization, while the media were rinsed and the abrasive paste renewed. The paste was renewed every hour because, due to the impacts between the media, it shatters during the finishing process, shifting its grain size distribution towards smaller values and therefore losing its abrasive capacity.

2.3 Characterization

The microstructure at the core of as-sintered, solution-annealed, and thermally aged specimens was observed by light Optical Microscopy (OM, Nikon Eclipse LV150NL) and by Field-Emission Scanning Electron Microscopy (FE-SEM, Zeiss SIGMA 500) equipped with a spectrometer for Energy Dispersive X-Ray Spectroscopy (EDX, Oxford Ultim Max). The samples were prepared according to usual metallographic procedures: grinding, polishing, and chemical etching with Kalling I reagent. The microhardness of the samples ($HV_{0.3}$) was tested by Vickers indentation with a load of 300 g_f for 15 s (FM-180, Future Tech). Roughness linear parameters (Ra, Rq, Rt, Rv, Skewness and Kurtosis) were measured with a contact profilometer (Formtracer Avant, Mitutoyo) with a measuring length of 4.0 mm and a cut-off of 0.8 mm. Measurements were repeated on the same sample five times to guarantee high accuracy and were performed along two perpendicular directions, namely, X and Y. Surface texture parameters and 3D reconstructions were obtained with a confocal optical profilometer (NPS, Hirox) with a surface scan of 1 mm^2 and a cut-off of 0.8 mm. Surface morphology after mass finishing was investigated by Scanning Electron Microscopy and Energy Dispersive X-Ray Spectroscopy (Phenom XL G2, Thermo Fisher Scientific). Mass loss was monitored using an analytical scale ADA 120/C (±0,0001 g). The density of sintered samples was evaluated by Archimedes' method, employing an analytical scale (XPR 105, Mettler Toledo).

3 Results and discussion

3.1 Material comparison between the as-sintered and thermally treated conditions

The internal microstructures of as-sintered, solution-annealed, and thermally aged (H900) specimens are shown in Fig. 2a, b, and c, respectively. A qualitative analysis reveals common features that remain unchanged during the different stages of the thermal

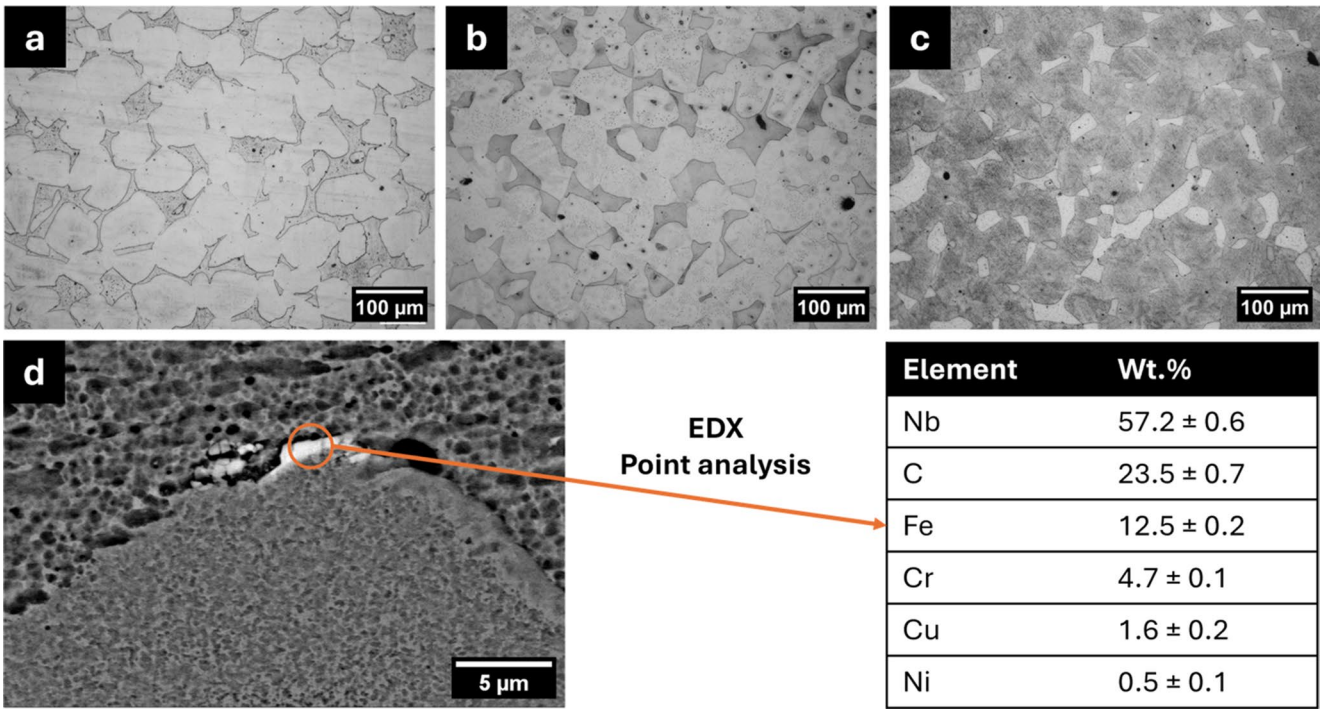

Element	Wt.%
Nb	57.2 ± 0.6
C	23.5 ± 0.7
Fe	12.5 ± 0.2
Cr	4.7 ± 0.1
Cu	1.6 ± 0.2
Ni	0.5 ± 0.1

Fig. 2 Light optical micrographs of **a**) as-sintered, **b**) solution-annealed, and **c**) aged (H900) specimens; **d**) EDX analysis of an inclusion at a grain boundary of the H900 specimen

process. Indeed, in all cases, the bulk material is characterized by an α' martensitic matrix, as also observed in other studies [44, 45]. This matrix is surrounded by a δ ferrite network, formed at the peak sintering temperature, which is stable at both the solution annealing and aging temperatures. The presence of extended grain boundaries among these constituents favors the nucleation and growth of secondary phases, such as niobium carbide with the typical elongated prismatic shape (Fig. 2d) already observed in previous studies on 17-4PH components by AM [2, 46]. The sintered samples have a relative density exceeding 95% of the nominal density (H: 96.51 ± 0.40%, O: 96.16 ± 0.25%, and V: 96.65 ± 0.17%) with spherical and closed porosity distributed in the material. $HV_{0.3}$ decreases from 277.4 ± 3.9 to 262.4 ± 12.3 after solution annealing and then increases to 396.4 ± 22.9 after thermal aging. The microhardness is controlled primarily by the presence of copper precipitates and, secondarily, by the tempering of martensite. As expected, the solubilization effectively removed copper precipitates and coarse inclusions formed during the cooling process after sintering, thus reducing the hardness of the martensitic grains. The H900 cycle, on the other hand, promotes the nucleation of fine and coherent BCC precipitates in the α' matrix, which limits the dislocation mobility within the martensite grains and strengthens the whole material.

3.2 Mass finishing optimization for the as-sintered samples

As-sintered specimens exhibit a rough morphology, characterized by cavities and surface porosity, as shown in Fig. 3a. The orientation relative to the printing plane influences the extent of surface defects and the initial roughness values: as expected, H-upskin surfaces appear more compact and show lower roughness. However, for the H orientation, a significant difference is observed between upskin surfaces (Ra = 5.38 ± 0.59 µm) and downskin surfaces (Ra = 8.68 ± 1.51 µm). The most unfavorable conditions correspond to the O-oriented samples, whose initial roughness ranges from Ra = 7.5 µm to Ra = 10.3 µm, in the upskin (Y direction) and downskin (X direction) surfaces, respectively. Instead, the difference between upskin and downskin is minimal, with average roughness values of Ra = 8.90 ± 1.17 µm and Ra = 8.15 ± 0.54 µm, respectively. Vertical surfaces exhibit an intermediate roughness in comparison with the previously discussed orientations (Ra = 7.61 ± 0.41 µm). Additionally, they show the smallest difference between the measurement directions parallel and perpendicular to the printing plane (less than 4%). For these reasons, for the sake of space and simplicity, in the following section, we present only surface morphologies and topographies of vertically oriented samples; roughness data are instead reported for all orientations.

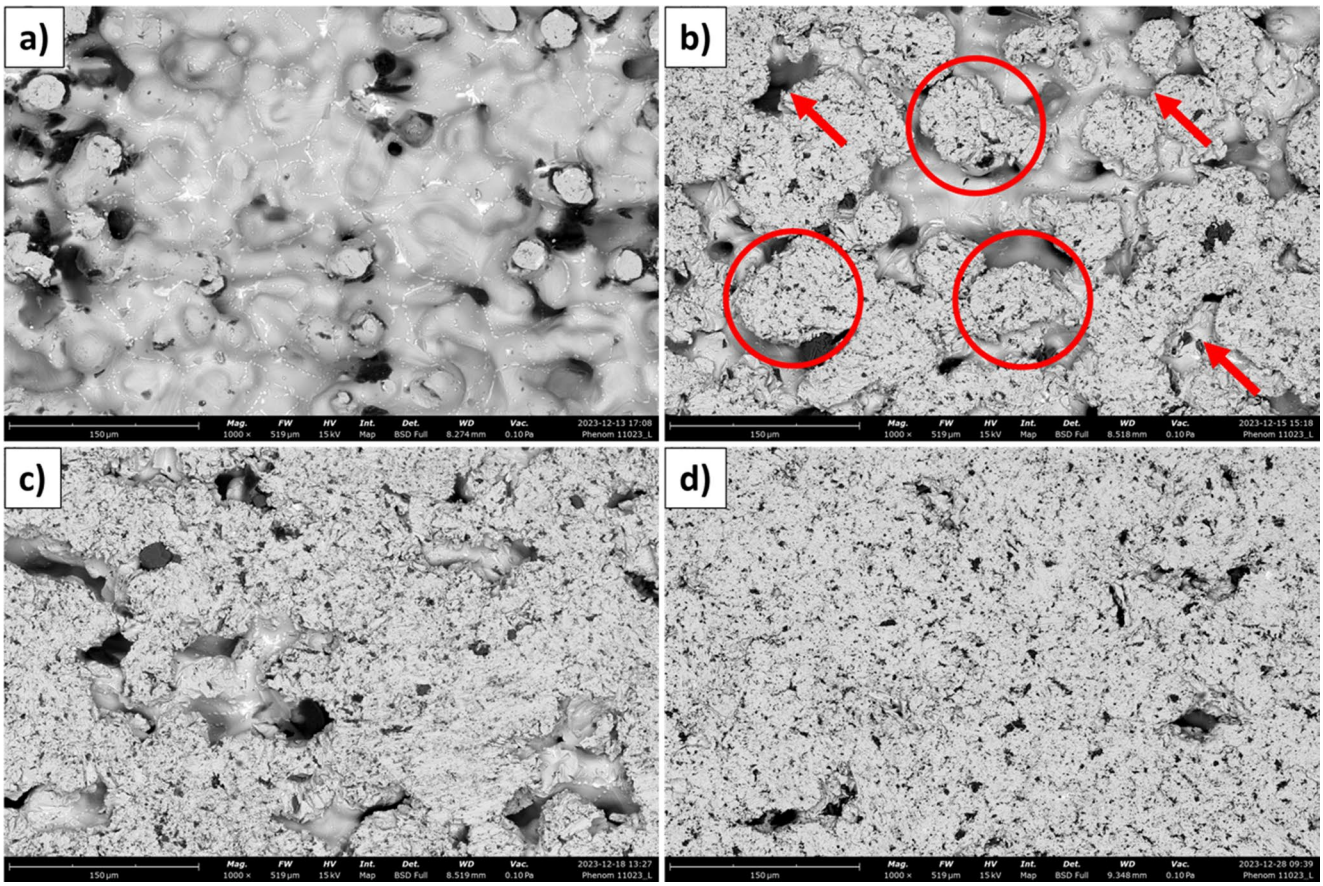

Fig. 3 SEM surface morphologies of **a**) as-sintered 17-4PH, and SiC mass finished surfaces after **b**) 1 h, **c**) 2 h, and **d**) 4 h

The mass finishing process has proven to be effective in reducing roughness and homogenizing the surface. After 4 h of treatment, a roughness reduction exceeding 60% was recorded on all surfaces, regardless of the abrasive media used. The most effective process corresponds to the highest mass loss rate (RSP 587, with an average of 29 mg/h), leading to final roughness values ranging between Ra = 0.26 µm and Ra = 1.14 µm, depending on the surface orientation (average among different orientations: Ra = 0.62 ± 0.25 µm and ΔRa = -92.08%). During mass finishing, the mechanical action of the media removes asperities, progressively forming smoother planes whose extent increases with treatment duration (Figs. 3b-d and 4b-d). On the contrary, the mechanical action of the abrasive paste and media does not reach the deep valleys and porosities of the material until an advanced stage of the mass finishing process. Figure 3 shows morphological changes of the V sample treated with SiC-based abrasive paste as a function of process time. After the first hour, when the highest peaks are reduced, flat islands (highlighted with red circles) and deep valleys (highlighted with red arrows) start to form (Figs. 3b and 4b). The three-dimensional reconstruction of the surface (Fig. 4) supports the interpretation of the SEM analyses: the areas circled in red showing micro-scratches are those smoothed by the abrasive action of the media; the areas indicated by the red arrows, in which it is possible to recognize the morphology of the as-sintered sample, are valleys not involved by the abrasive action of the media. The formation of flat areas following the removal of material from asperities is the typical leveling mechanism developed in mass finishing processes [19, 27, 31]. These wide topographical depressions are still present until the third hour of the process. After four hours, the surface is completely levelled, and a few pores remain with dimensions ranging from about 10 µm to 40 µm. The effectiveness of the treatment decreases over time, as the amount of material removal required for roughness reduction increases. This trend is evident from the evolution of the Rp and Rv parameters reported in Table 1: the former decreases predominantly within the first hour of the process (on average, $\Delta Rp\ (1\ h) \approx -75\%$ for the test with RSP 587), while the latter decreases more gradually until it stabilizes at values between Rv = 1.96 µm (H upskin, along Y direction) and Rv = 11.24 µm (O upskin, along Y direction). At the end of the process, the surface appears flat with valleys

corresponding to areas where the abrasive action is ineffective. The initially homogeneous profile distribution (for the vertical orientation: Rp = 21.76 ± 2.10 µm, Rv = 23.32 ± 2.42 µm, Rsk = 0.07 ± 0.13 along X direction and Rsk = − 0.01 ± 0.03 along Y direction for the test with RSP 587) during the process shifts toward a valley-dominated profile, reaching an Rsk value of – 2.42 ± 0.35 along X direction, and of – 3.05 ± 0.41 along Y direction. Similarly, regarding the kurtosis (Table 1), normal height distribution of the as-sintered samples (Rku close to 3), shifted toward a spiked distribution upon mass finishing treatment: this highlights the effectiveness in peaks smoothening, resulting in flat surfaces with few small deep valleys. The density of valleys is inversely proportional to both the processing time and the material removal rate (see micrographs or 3D reconstructions reported in Fig. 4).

3.2.1 Effect of abrasive pastes

Figure 5 compares V-samples morphology before and after four hours of mass finishing with the three abrasive pastes, while Fig. 6 shows their surface topography, and Fig. 7 shows

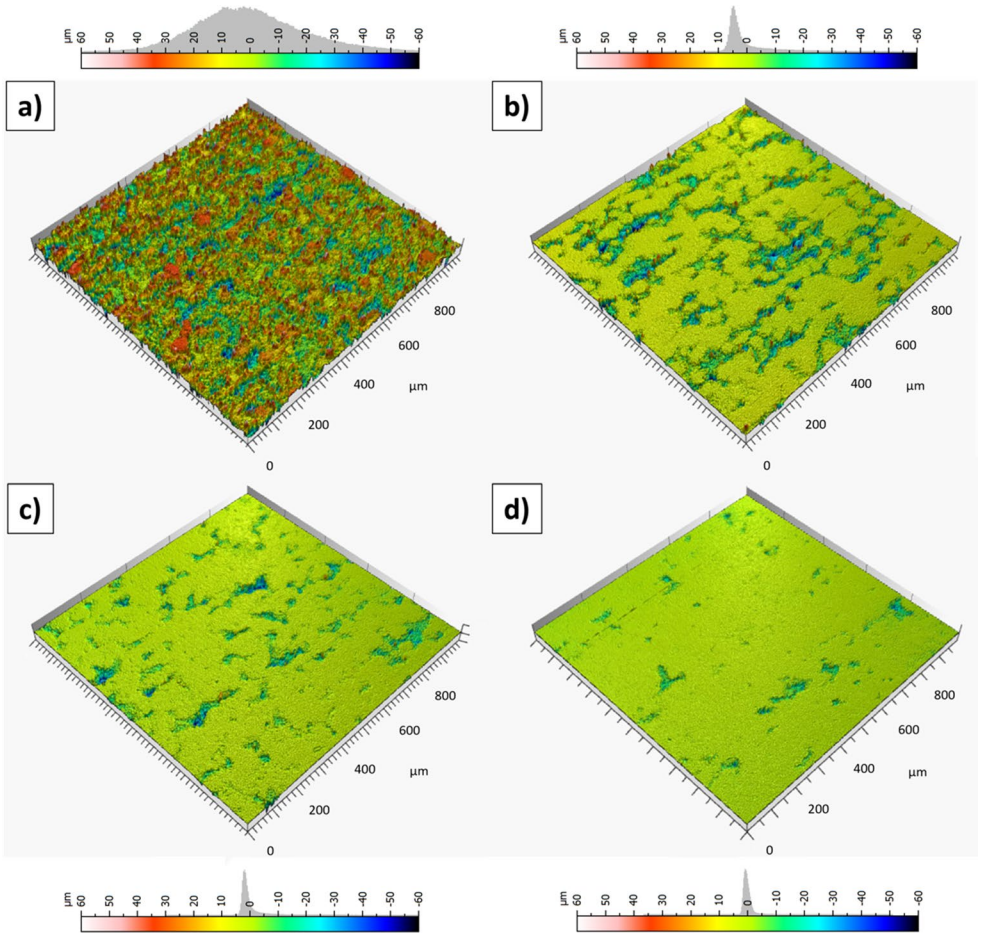

Fig. 4 Surface topographies of **a**) as-sintered 17-4PH, and SiC mass finished surfaces after **b**) 1 h, **c**) 2 h, and **d**) 4 h

Table 1 Relevant roughness parameters in the as-printed condition (*initial*) and after 4 h of mass finishing (*final)* with SiC-based abrasive paste on the as-sintered horizontal (H), vertical (V), and oblique (O) samples

	SiC on as-sintered 17−4 PH								
	Horizontal (up - X)			Vertical (X)			Oblique (down - X)		
	Initial (µm)	Final (µm)	Variation (%)	Initial (µm)	Final (µm)	Variation (%)	Initial (µm)	Final (µm)	Variation (%)
Rq	6.81	0.40	-94.12	9.50	1.06	-88.84	9.31	1.35	-85.50
Rz	31.87	2.50	-92.15	45.10	6.33	-85.96	40.36	7.34	-81.83
Rp	16.01	0.49	-96.94	21.76	0.83	-96.18	20.98	1.00	-95.23
Rv	15.86	2.01	-87.32	23.34	5.44	-76.70	19.38	6.34	-67.32
Rsk	0.11	-1.95	-1890.9	0.07	-2.42	-3632.2	0.15	-2.56	-1829.4
Rku	3.15	9.65	206.18	2.57	11.36	342.16	2.55	12.85	403.03

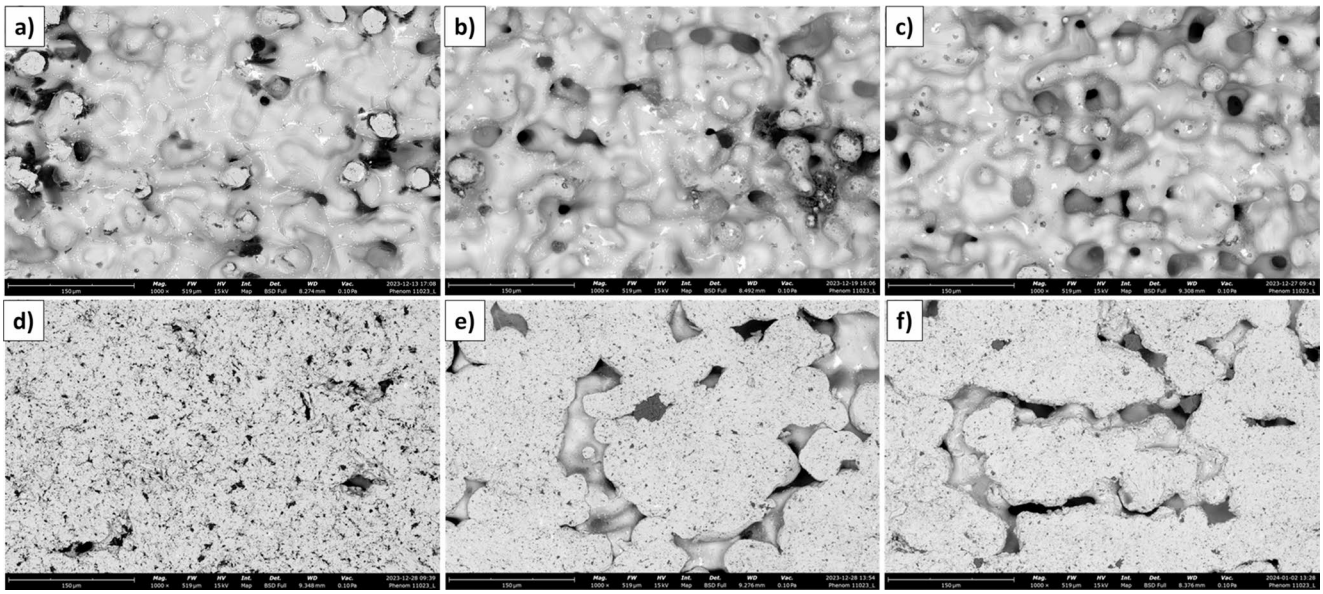

Fig. 5 SEM morphologies of three as-sintered 17-4PH V-samples before (**a**, **b**, **c**) and after mass finishing for 4 h with **d**) SiC, **e**) Al_2O_3, and **f**) SiO_2 abrasive pastes

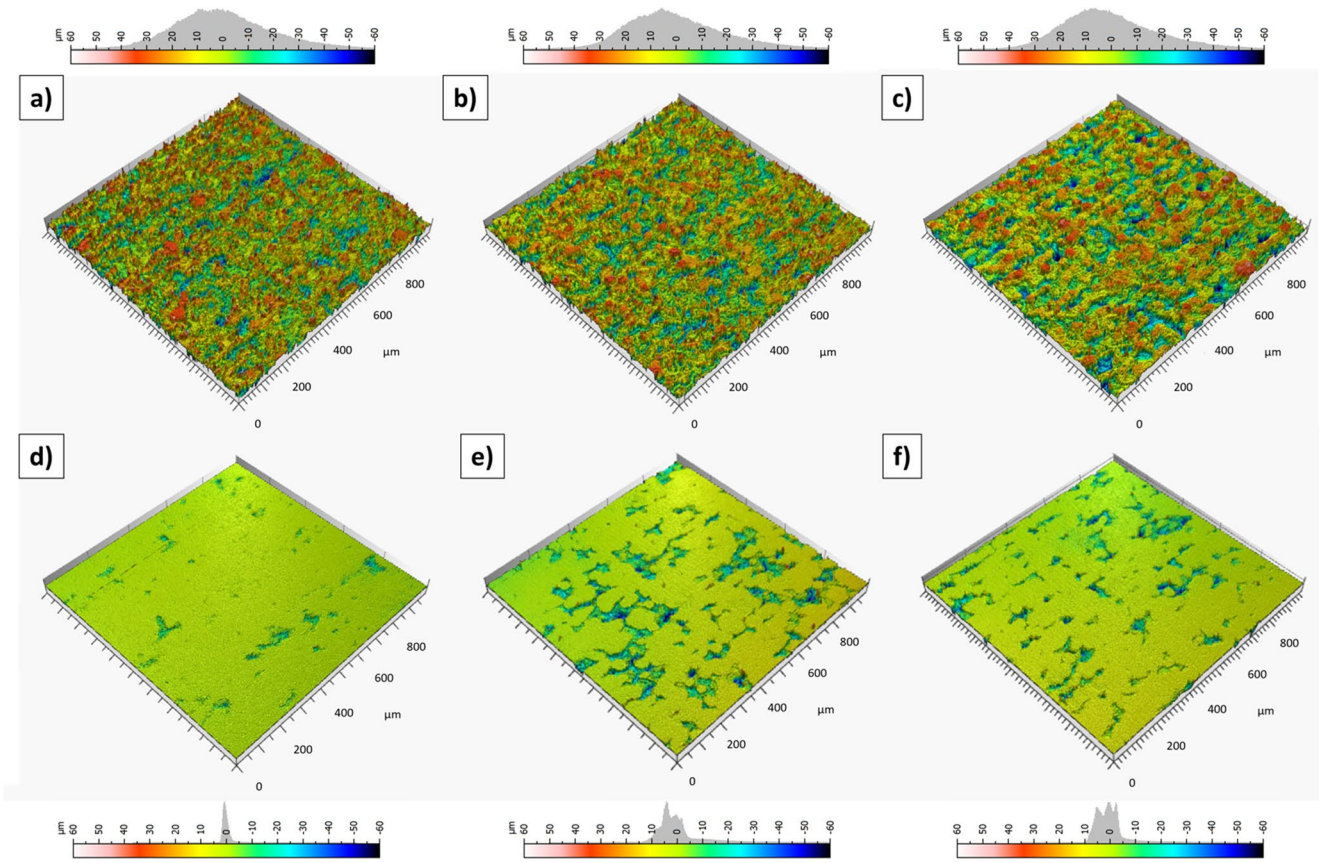

Fig. 6 Surface topographies of three as-sintered 17-4PH V-samples before (**a**, **b**, **c**) and after mass finishing for 4 h with **d**) SiC, **e**) Al_2O_3, and f) SiO_2 abrasive pastes

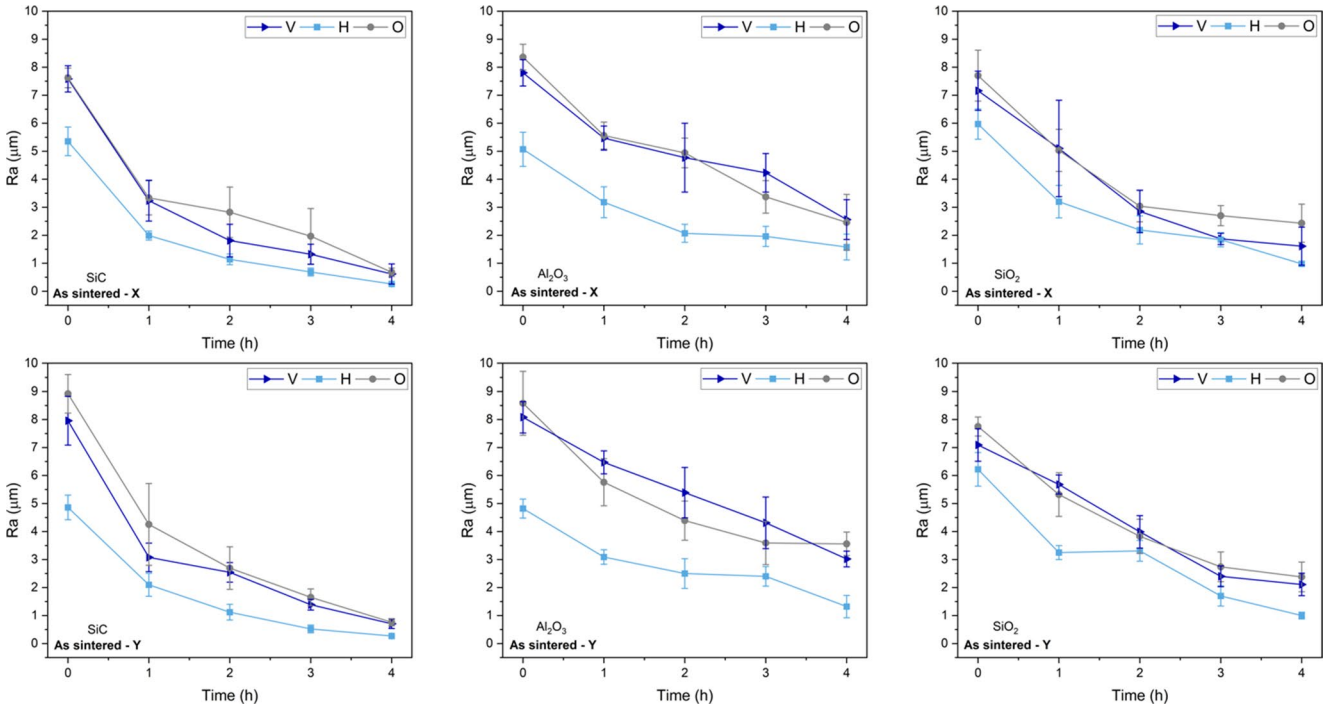

Fig. 7 Average surface roughness (Ra) of as-sintered samples as a function of mass finishing time for the different abrasive pastes. The measured surfaces were of a V-sample, H-upskin sample, and O-downskin sample

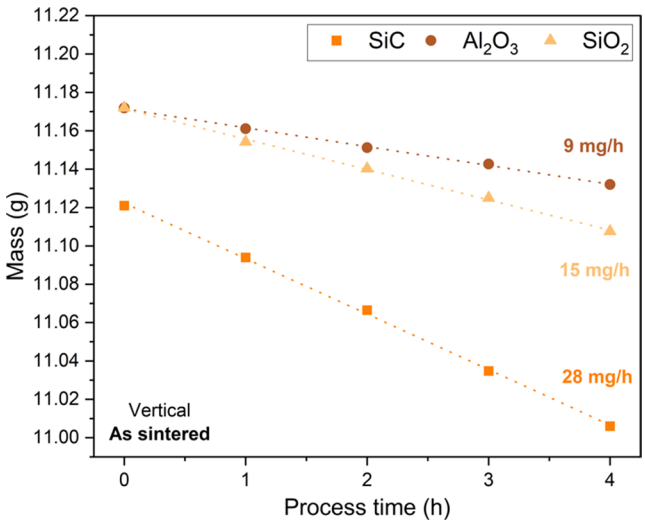

Fig. 8 Mass loss measured on the as-sintered V-samples as a function of time for the different abrasive pastes (i.e., SiC, Al_2O_3, and SiO_2)

the roughness variation during mass finishing. The sample treated with SiC-containing paste presents a smoother and defect-free morphology than those treated with Al_2O_3- and SiO_2-containing pastes. Its surface appears homogeneously flattened, while samples treated with Al_2O_3- and SiO_2-containing pastes present similar surfaces with alternating planes and valleys. This difference can be correlated with material removal rates and roughness variation (Figs. 8 and 9): the SiC-based paste removed about twice as much material as the SiO_2-containing paste and about three times as much material as the Al_2O_3-containing paste. As a matter of fact, morphologies of samples treated with Al_2O_3- and SiO_2-containing pastes after four hours of process resemble that of samples treated with SiC-containing paste after two hours of treatment, as shown in Fig. 3. When comparing the mass loss measured on samples treated using the same abrasive paste, material removal rate variations among samples printed with different orientations was lower than 3%, highlighting that the small density differences among H, V, and O samples (Section 3.1) did not affect the finishing outcome. Therefore, the mass finishing process was apparently more influenced by morphological features correlated to surface orientation rather than by sintering defects. Roughness measurements further highlight these differences (Figs. 6 and 8): in the case of SiC-based paste, the roughness significantly decreased in the first hour of the process ($\Delta Ra/\Delta t = -4.35$ μm/h for V-sample along X direction and $\Delta Ra/\Delta t = -4.88$ μm/h for V-sample along Y direction) and decreased more slowly afterward in the following three hours ($\Delta Ra/\Delta t = -0.87$ μm/h for V-sample along X direction and $\Delta Ra/\Delta t = -0.79$ μm/h for V-sample along Y direction). For the other two abrasives, roughness variations occurred more gradually: concerning Al_2O_3-based paste, $\Delta Ra/\Delta t$ in the first hour of the process are – 2.33 μm/h and −1.61 μm/h for V-sample along X and Y direction, respectively; in the following three hours they are – 1.31 μm/h and – 1.27 μm/h along X and Y direction, respectively. Concerning SiO_2-based paste, $\Delta Ra/\Delta t$ in the

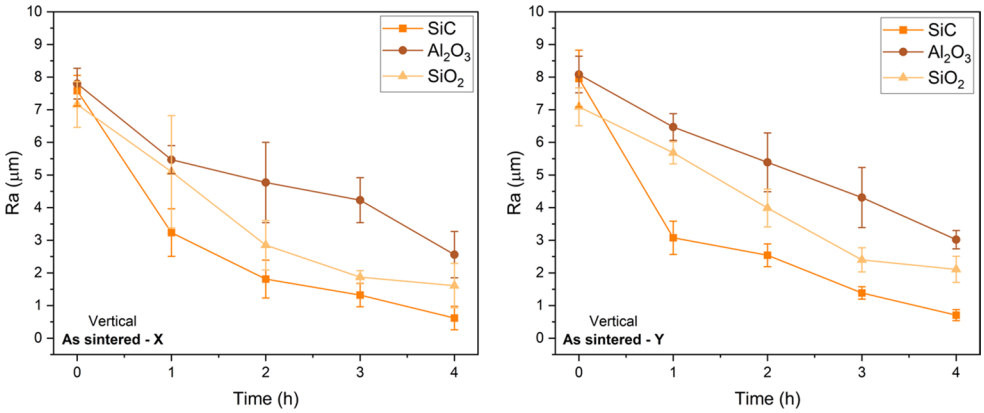

Fig. 9 Comparison of the average surface roughness of as-sintered V-samples on the X and Y directions, measured as a function of time for different abrasive pastes (i.e., SiC, Al_2O_3, and SiO_2)

Table 2 Relevant roughness parameters in the as-printed condition (*initial*) and after 4 h of mass finishing (*final)* with Al_2O_3-based abrasive paste on as-sintered horizontal (H), vertical (V), and oblique (O) samples

	Al_2O_3 on as-sintered 17−4 PH								
	Horizontal (up - X)			Vertical (X)			Oblique (down - X)		
	Initial (μm)	Final (μm)	Variation (%)	Initial (μm)	Final (μm)	Variation (%)	Initial (μm)	Final (μm)	Variation (%)
Rq	6.43	2.32	−63.9	9.81	3.66	−62.69	10.30	3.70	−64.08
Rz	30.06	12.02	−60.01	44.84	18.34	−59.10	44.73	19.17	−57.14
Rp	14.12	1.88	−86.68	23.14	3.59	−84.48	21.46	3.44	−83.97
Rv	15.94	10.14	−36.38	21.70	14.75	−32.03	23.27	15.73	−32.40
Rsk	-0.03	-2.34	7211.3	0.09	-2.07	-2366.2	-0.09	-2.67	2945.9
Rku	2.91	8.63	196.34	2.88	8.21	185.3	2.65	11.48	333.79

Table 3 Relevant roughness parameters in the as-printed condition (*initial*) and after 4 h of mass finishing (*final)* with SiO_2-based abrasive paste on as-sintered horizontal (H), vertical (V), and oblique (O) samples

	SiO_2 on as-sintered 17−4 PH								
	Horizontal (up - X)			Vertical (X)			Oblique (down - X)		
	Initial (μm)	Final (μm)	Variation (%)	Initial (μm)	Final (μm)	Variation (%)	Initial (μm)	Final (μm)	Variation (%)
Rq	7.45	1.64	−77.99	8.77	2.44	−72.18	9.36	3.58	−61.75
Rz	35.37	9.34	−73.59	38.00	13.15	−65.39	40.13	17.70	−55.89
Rp	17.15	1.40	−91.84	17.45	2.48	−85.79	18.31	3.31	−81.92
Rv	18.22	7.95	−56.37	20.55	10.67	−48.08	21.82	14.39	−34.05
Rsk	-0.06	-2.71	4617.4	-0.16	-2.19	1248.0	-0.14	-2.25	1479.1
Rku	2.93	13.16	348.67	2.60	10.11	288.28	2.62	9.13	248.33

first hour of the process are – 2.06 μm/h and – 1.41 μm/h for V-sample along X and Y direction, respectively; in the following three hours, they are – 1.39 μm/h and – 1.25 μm/h along X and Y direction, respectively. On average among the ten considered directions, Ra decreased to 0.62±0.25 μm with SiC-paste, to 1.79±0.62 μm with SiO_2-paste and to 2.69±0.78 μm with Al_2O_3-paste.

Moreover, considering roughness parameters reported in Tables 1 and 2, and 3, the effect of different abrasives can be further clarified. Rp decreases differently according to surface orientation: the H-upskin is always smoother than the V and O-downskin surfaces. Concerning SiC-based pastes, Rp is always reduced to less than 1 μm, reaching 0.49 μm in most favorable conditions (Table 1). For Al_2O_3 and SiO_2-based pastes, instead, Rp is decreased to values ranging between 1 μm and 2 μm on H-upskin surfaces and to values between 2.5 μm and 3.5 μm on the other surfaces (Tables 2 and 3). This behavior demonstrates the reduced wear efficiency of these pastes.

Regarding Rv, its reduction is limited to around −30% for Al_2O_3-containing paste (Table 2): this reflects on ΔRz, whose average reduction is around −60%. Both values are considerably lower compared to variations obtained with SiC-containing paste (Table 1). SiO_2-based paste shows an intermediate behavior (Table 3): Rv is significantly reduced in most favorable conditions (ΔRv=−56.37% on H-upskin along the X direction) and only partially reduced in the roughest orientation (Rv = -34.05% on O-downskin along the X direction). This difference reflects on Rz, which reaches values lower than 10 μm in the former case and higher than 17 μm in the latter.

Rq behaves like Ra, whose average variations over all tested conditions are – 92.29 ± 1.94% for SiC-based paste, − 76.32 ± 6.34% for SiO_2-based paste, and – 66.30 ± 4.94% for Al_2O_3-based paste. Finally, Rsk and Rku for Al_2O_3- and SiO_2-based pastes present a spiked height distribution shifted towards peaks, as for SiC-based paste: this is a general trend of mass finishing processes that remove material only from asperities, leaving flat surfaces characterized by wide planes and few valleys.

3.2.2 Effect of surface orientation

The morphological and roughness differences observed in the as-sintered specimens are reflected in the treated surfaces. In particular, the H-upskin orientation exhibits the lowest final roughness among all processes, achieving a minimum Ra = 0.26 µm in the SiC test along the X direction. Conversely, the O orientation remains the most unfavorable condition: during processing, the layered structure characteristic of the manufacturing process becomes evident, negatively impacting the roughness, particularly along the Y direction. After the mass finishing process, surface homogeneity generally improved. Differences between X and Y directions (Δ_{XY}, defined as $\Delta_{XY} = |Ra\ (X) - Ra\ (Y)|$) and upskin and downskin surfaces (Δ_{UD}, defined as $\Delta_{UD} = |Ra\ (upskin) - Ra\ (downskin)|$) on the same sample were considered. On average, for the as-sintered samples $\Delta_{XY} = 1.52$ µm and $\Delta_{UD} = 2.45$ µm. These values are reduced to 0.13 µm and 0.24 µm in the case of SiC-based paste, to 0.64 µm and 0.86 µm in the case of Al_2O_3-based paste, and to 0.41 µm and 0.47 µm in the case of SiO_2-based paste. The reduction of these parameters demonstrates an improvement in surface homogeneity. This trend can be correlated with differences in material removal rate, as already discussed for other roughness parameters.

3.2.3 Compositional analysis

EDX analysis highlights the presence of residues of abrasive pastes and media on the surface after mass finishing. Figure 10 displays Si, C, and Al elemental distribution on the samples treated with SiC-based paste: residues smaller than 1 µm are distributed all over the surface, while larger particles (with a dimension of around 10 µm) get stuck in correspondence of deep valleys. The presence of Si is attributed to the main component of abrasive paste (SiC): during the treatment, abrasive particles are ground by media pressure and reduce their size, shifting the granulometric distribution towards lower values. The presence of carbon can be attributed to the SiC paste, to environmental contamination, and to C presence as an alloying element in the 17-4PH alloy. Al comes from Al_2O_3, a minor component in the abrasive paste RSP 587. Similar conclusions can be drawn for samples treated with other pastes: small traces, attributable to media or abrasive pastes, were revealed on all samples. As surface roughness increases, the possibility of finding macroscopic residues embedded in the porosities and valleys increases as well.

Observed paste residues do not compromise components biocompatibility. According to ISO 10,993 standards [47] for biological evaluation of medical devices, biocompatibility requirements depend on both the type and duration of tissue contact. In the case of surgical instruments with transient exposure to bone and soft tissues, surface residues of inert compound such as SiC, and stable oxides like SiO_2 and Al_2O_3 are not considered critical. These compounds are widely used in polishing protocols for biomedical alloys and are recognized for their chemical stability and lack of cytotoxic or inflammatory response in clinical applications [48].

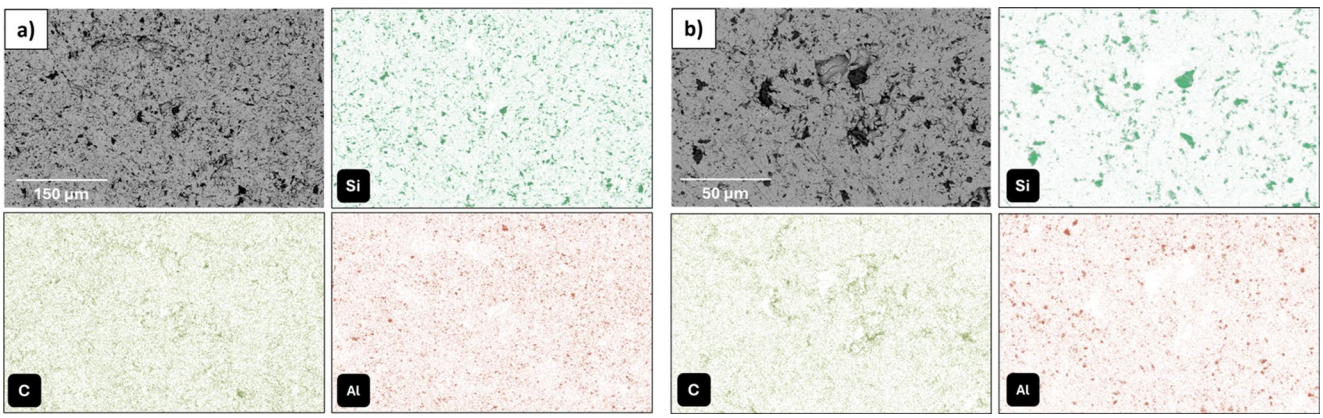

Fig. 10 SEM micrographs at different magnifications, with (**b**) focusing on the highlighted area of (**a**), of the 17-4PH as-sintered sample after 4 h mass finishing (SiC-based paste), with corresponding EDX maps for silicon, carbon, and aluminum

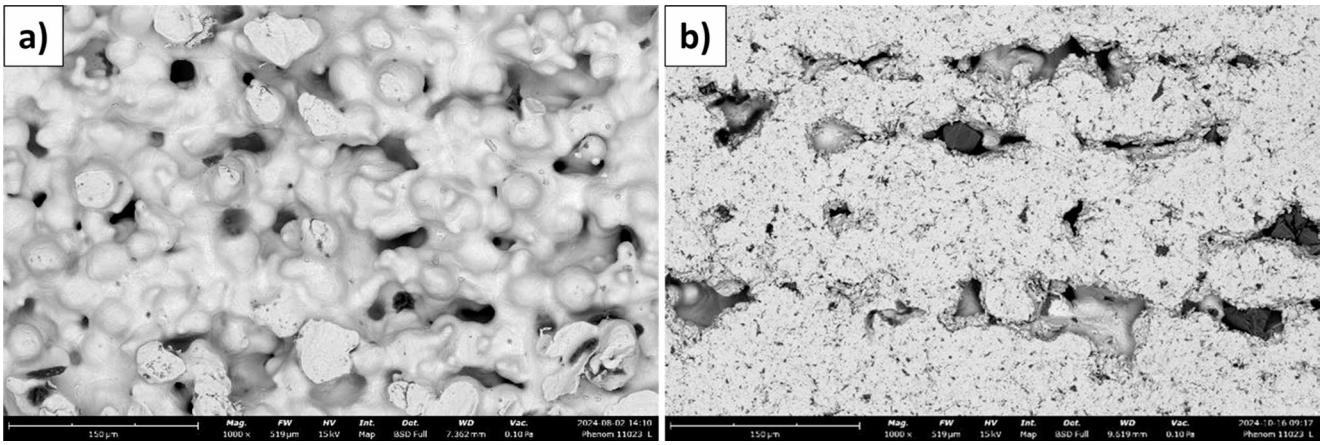

Fig. 11 SEM morphologies of H900 samples printed in the vertical orientation **a**) before mass finishing and **b**) after 4 h of SiC abrasive treatment

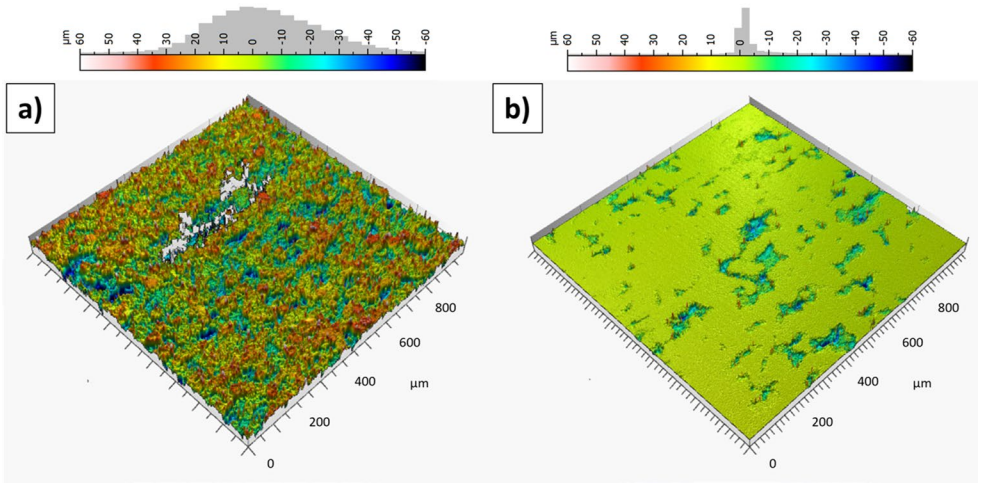

Fig. 12 Surface topographies of H900 samples printed in the vertical orientation **a**) before mass finishing and **b**) after 4 h of SiC abrasive treatment. White areas in the picture on the left correspond to points out of the measuring range

3.3 Comparison of SiC mass finishing on the as-sintered and H900 samples

The most effective finishing process was repeated on the thermally treated material. Samples employed for the thermal aging belonged to a different printing batch and therefore their initial roughness differed from that of the samples used for the optimization mass finishing process (Section 3.2). The mass finishing efficiency and efficacy was quantified in terms of roughness decrease rate and mass loss, thus the initial difference in surface quality was not believed to affect the overall evaluation. SiC-based paste effectively smoothened the specimen surface, as shown in Figs. 11 and 12 for the V samples. Additional SEM images showing surface morphological evolution of the H and O specimens are reported in Supplementary Materials. The average final value of Ra = 1.80 ± 0.91 µm, corresponding to an average reduction of ΔRa (4 h) = − 81.1%, was obtained on the different surface orientations. Figure 13 shows the roughness change during the SiC mass finishing process for the different orientations of thermal-aged samples. Reductions were lower compared to those obtained in the same conditions on untreated samples (final average Ra = 0.62 ± 0.26 µm; ΔRa (4 h) = − 92.2%): the reduced process efficiency can be correlated with the lower material removal rate experienced on the thermally treated samples (Fig. 14). After thermal treatment the hardness increased (ΔHV = + 42.9%), improving material abrasion resistance: a reduced thickness of material was removed, leading to the formation of smaller flat islands, alternated by deep valleys (average Rz after 4 h was 5.62 µm and 12.67 µm, for the as-sintered and H900 aged material, respectively). Similar conclusions can be drawn considering surface morphologies (Fig. 11): in the first hour of the process, few planes were formed, and most of the surface looked similar to the as-sintered one. In the following hours, planes widened, and valleys width reduced. However, after four hours, the valleys width remained between 20 and 50 µm. Reduced smoothening was found on the sample with H-downskin orientation, where initial roughness was higher: the lowest ΔRa (4 h) was measured (on average – 73.0% along X direction, and – 67.9% along Y direction), resulting in a final Ra exceeding 3 µm. The reduced efficacy of this orientation was most probably due to the

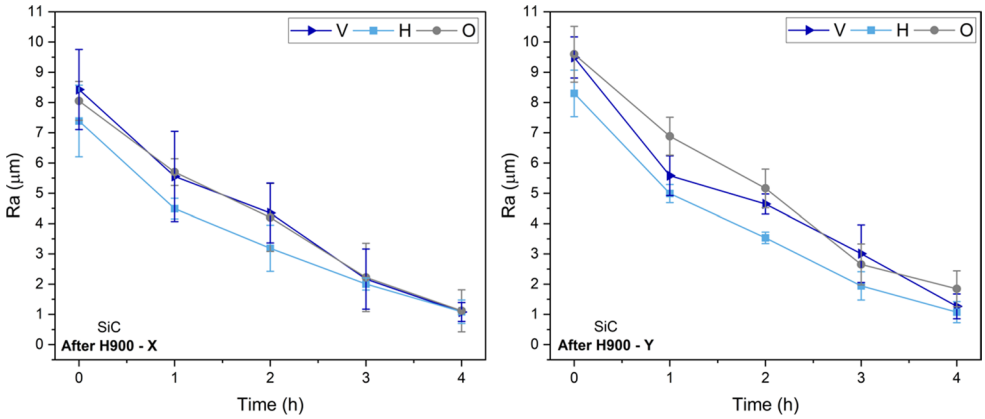

Fig. 13 Average roughness (Ra) of H900 aged as a function of mass finishing time with SiC abrasive paste and measured on X and Y directions for the V sample, H-upskin surface, and O-downskin surface

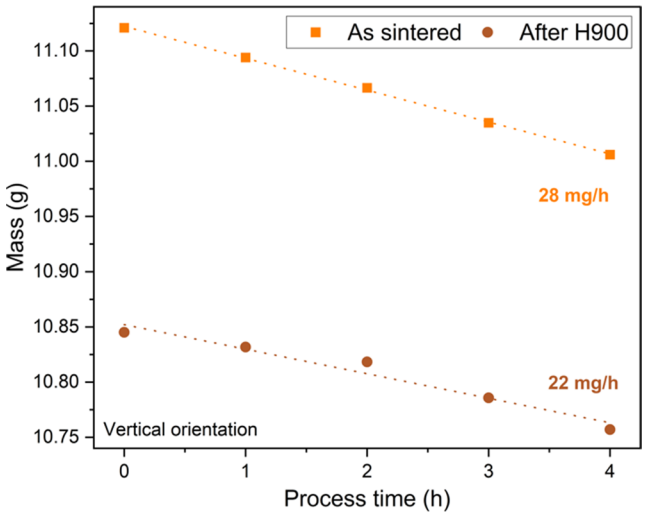

Fig. 14 Mass loss measured on as-sintered and H900 V-samples as a function of time during SiC mass finishing

anomalous initial roughness of the sample, much higher than the others. Concerning other orientations, samples presented ΔRa (4 h)≥80% (83.7% on average), with the only exception of O-upskin along X direction, corresponding to final Ra between 1 and 2 µm. Thermally treated samples exhibited a more uniform decrease in surface roughness over time compared with the as-printed ones (Fig. 13), with an average ΔRa/Δt=1.84 µm/h and 2.06 µm/h for V-sample along X and Y directions, respectively. In the first hour of the test, roughness reduction was slightly higher compared to the following three hours: for V-samples along the X direction, ΔRa/Δt (1 h) was 2.87 µm/h and average ΔRa/Δt in the following three hours was 1.49 µm/h; along the Y direction it was 3.91 µm/h in the first hour and 1.44 µm/h in the following three hours. This behavior is different with respect to that observed on as-sintered samples polished with SiC-based paste, that underwent a significantly higher roughness reduction in the first hour of the process and a limited reduction afterward. Based on this observation, a further roughness reduction may be expected on thermally treated samples by extending process time: in particular, Ra values similar to those of the as-sintered samples can be obtained with only one additional processing hour. From Table 4, it can be observed that the reduction of Rp on thermally treated samples is significantly lower than on as-sintered ones: Rp remained higher than 1 µm (even higher than 2 µm in less favorable conditions) on thermally treated surfaces, while it was always reduced below 1 µm on as-sintered samples. Since Rp was not as low as in the case of as-sintered samples, by increasing processing time a further reduction of roughness is expected. Deep valleys remained on polished thermally treated surfaces, as shown by surface topography (Fig. 12), with Rv values ranging from 5 to 10 µm. As already mentioned, these sites may easily trap residues from media or abrasive pastes. The limited variations of Rp and Rv affected the improvement of Rz and Rq, Rz being

Table 4 Relevant roughness parameters in the as-printed condition (*initial*) and after 4 h of mass finishing (*final)* SiC-based abrasive paste on thermally aged (H900) horizontal (H), vertical (V), and oblique (O) samples

	SiC on hardened 17−4 PH								
	Horizontal (up - X)			Vertical (X)			Oblique (down - X)		
	Initial (µm)	Final (µm)	Variation (%)	Initial (µm)	Final (µm)	Variation (%)	Initial (µm)	Final (µm)	Variation (%)
Rq	9.10	1.69	−81.43	10.57	1.79	−83.07	10.07	2.06	−79.54
Rz	41.87	9.21	-78.00	50.01	10.32	−79.36	45.74	11.30	−75.29
Rp	21.26	1.49	−94.14	24.11	1.40	−94.19	21.95	2.04	−90.71
Rv	20.61	7.72	−62.54	25.90	8.92	−65.56	23.78	9.25	−61.10
Rsk	0.16	-2.53	-1710.6	0.05	-3.23	-6283.0	-0.04	-2.30	5897.4
Rku	2.75	10.81	292.37	2.92	16.50	464.69	2.90	11.47	295.48

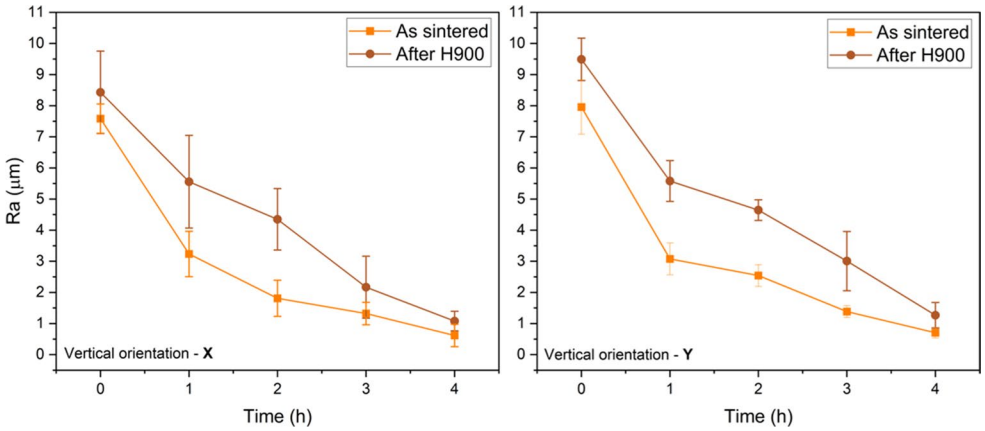

Fig. 15 Comparison of the average surface roughness of as-sintered and H900 V-samples on the X and Y directions, measured during SiC mass finishing

more affected by the presence of a few deep valleys. Finally, Rsk and Rku have a spiked height distribution and shifted towards peaks, as for as-sintered samples.

Figure 14 shows the mass loss measured on as-sintered and H900 V-samples as a function of treatment time. The average slopes of the profile were 28 and 22 mg/h for the untreated and hardened conditions, respectively. Figure 15 compares the average roughness change along X and Y directions. In contrast with the mass loss, the difference between the as-sintered and thermally treated conditions is not so evident, at least visually. In fact, after 4 h of finishing on V-sample, the Ra is lowered by 91.9% on the as-sintered material while by 87.2% on the thermally hardened steel (X-direction).

The mass finishing performance was influenced by the specimen hardness and by the inherent variability of the BJT printing quality. The roughness of the thermally aged material decreases more slowly than that of the as-sintered one. Since it is reasonable to consider that the roughness is not altered by the thermal treatment, we conclude that it is preferable to perform the mass finishing before the thermal aging, to meet the roughness requirements in a shorter time.

4 Conclusions

Binder Jetting (BJT) is an AM technology that allows for producing 17-4PH steel components characterized by mechanical properties comparable to those obtained by conventional production techniques. It is of particular interest because of its high productivity and easy implementation within the powder metallurgy industry. Mass finishing is a well-established surface finishing technique at the industrial level, that reduces roughness by mechanical abrasion in a single-step process. Although it has already been exploited for post-processing of components produced by laser-based AM technologies, the literature still lacks a systematic investigation focused on the BJT finishing.

The present work optimized a mass finishing process for 17-4PH parts produced via BJT for the manufacturing of orthopedic surgical instruments, analyzing the surface characteristics of polished components before and after the precipitation hardening heat treatment. Specifically, the effect of three different abrasive pastes (namely SiC-, SiO_2-, and Al_2O_3-based pastes) was investigated on flat surfaces printed with different orientations. Surface morphologies and roughness parameters were monitored during the mass finishing process. The main findings of the study are listed as follows:

- Mass finishing has proven to be a valid process to address the surface finishing of components produced via BJT, complying with the functional requirements of the biomedical sector. By means of SiC-containing paste, lowest roughness was reached, with Ra = 0.62 ± 0.25 µm (average among the five different surfaces of interest) after 4 h of mass finishing in a centrifugal disk machine.
- Abrasive paste effectiveness was correlated with the material removal rate. The SiC-containing paste, which led to the highest material removal rate, provided the best surface smoothening.
- Traces of abrasive pastes, including micrometric residues of Si and Al, were detected on the surfaces. Being inert and confined to surface valleys, they do not raise biocompatibility concerns according to the ISO 10,993 [47].
- The roughness parameters and material removal rate of the as-sintered and thermally aged (H900) samples were compared, observing that the hardening of the steel lowers the finishing rate. Therefore, to obtain a similar Ra value to the as-sintered condition, it is necessary to extend the finishing time on thermally treated samples.
- Within the production cycle of additively manufactured orthopedic surgery instruments, it is preferable to perform the mass finishing process on the as-sintered components and proceed later with the thermal hardening of the material.

The present work succeeded in identifying a mass finishing process for BJT components able to obtain results compliant with requirements for the biomedical sector. Further tests on objects with real dimensions and geometries are necessary: the process has been developed limitedly to small components with simple shapes. It can be expected that when transferring the process to components of different sizes and geometries, modifications will be necessary, such as the choice of media that must be able to reach all surfaces of the components.

Overall, these findings support the integration of mass finishing into the production workflow of BJT-manufactured surgical instruments, enabling improved surface quality without compromising process efficiency.

Supplementary Information The online version contains supplementary material available at https://doi.org/10.1007/s00170-026-18334-9.

Funding Open access funding provided by Politecnico di Milano within the CRUI-CARE Agreement. The project is funded under the "Fondo per la Crescita Sostenibile - Bando Accordi Innovazione DM 31/12/21 - DD 18/03/22 - Progetto PASO - Produzione Additiva di Strumentari Ortopedici, B49J23000620005, ID. 10188".

Data availability Data will be available upon reasonable request.

Declarations

Conflict of interest The authors declare they have no conflict of interest.

References

1. Zhao W, Chang J, Wei Q, Wu J, Ye C (2024) Effect of sodium silicate solution combined yttrium oxide stabilized zirconia nanopowders on the properties of alumina ceramics fabricated by binder jetting additive manufacturing. J Mater Process Technol 330:118454. https://doi.org/10.1016/j.jmatprotec.2024.118454
2. Salaheldin K, Abdelwahed M, Mariani M, Grande AM, Lecis N (2025) Effects of solution annealing and ageing treatments on the microstructure and mechanical properties of 17-4PH steel produced by binder jetting. Rapid Prototyp J 31(11):131–147. https://doi.org/10.1108/RPJ-08-2024-0332
3. Mao Y, Li J, Li W, Cai D, Wei Q (2021) Binder jetting additive manufacturing of 316L stainless-steel green parts with high strength and low binder content: Binder preparation and process optimization. J Mater Process Technol 291:117020. https://doi.org/10.1016/j.jmatprotec.2020.117020
4. Chen L, Chen W, Fu Z, Ding G, Chen Z, Zhu D (2023) Binder Jet 3D printing of 316L stainless steel: orthogonal printing and sintering process optimization. Adv Eng Mater 25(5):2200641. https://doi.org/10.1002/adem.202200641
5. Mirzababaei S, Pasebani S (2019) A review on binder jet additive manufacturing of 316L stainless steel. J Manuf Mater Process 3(3):82
6. Zheng S et al (2021) Implication of surface properties, bacterial motility, and hydrodynamic conditions on bacterial surface sensing and their initial adhesion. Front Bioeng Biotechnol 9:643722
7. Tandy J, Hanhquynh Le K, Deane GM (2022) Joseph Burns. Cleanability of metal surface finishes found in medical devices and the environment of care. Biomed Instrum Technol 56(2):29–36
8. Mostafaei A, Neelapu SHVR, Kisailus C, Nath LM, Jacobs TDB, Chmielus M (2018) Characterizing surface finish and fatigue behavior in binder-jet 3D-printed nickel-based superalloy 625. Addit Manuf 24:200–209
9. Lai W-J, Ojha A, Luo Z (2022) Effect of surface roughness on fatigue behavior of 316L stainless steel produced by binder jetting process. In: TMS 2022 151st Annual Meeting & Exhibition Supplemental Proceedings. The Minerals, Metals & Materials Series. Springer, Cham, pp 164–176. https://doi.org/10.1007/978-3-030-92381-5_15
10. Fan F, Jalui S, Shahed K, Mullany B, Manogharan G (2025) Mass finishing for additive manufacturing: Tribological analysis, surface topology, image processing, predictive model, and processing recommendations. Tribol Int 204:110486. https://doi.org/10.1016/j.triboint.2024.110486
11. Jamalkhani M, Nathan B, Heim M, Nelson D, Mostafaei A (2023) Fatigue behavior of vacuum-sintered binder jetted fine 316L stainless steel powder. Mater Sci Eng A 873:144937. https://doi.org/10.1016/j.msea.2023.144937
12. Atapour M, Wang X, Persson M, Odnevall Wallinder I (2020) Hedberg. Corrosion of Binder Jetting Additively Manufactured 316L Stainless Steel of Different Surface Finish. J Electrochem Soc 167(13):131503. https://doi.org/10.1149/1945-7111/abb6cd
13. Lores A, Azurmendi N, Agote I, Espinosa E, García-Blanco MB (2022) A study of parameter and post-processing effects on surface quality improvement of Binder Jet 3D-printed Invar36 alloy parts. Prog Addit Manuf 7(5):917–930. https://doi.org/10.1007/s40964-022-00267-w
14. Fabiocchi L, Mariani M, Lucchini Huspek A, Pozzi M, Bestetti M, Lecis N (2025) Low-energy high-current pulsed electron beam surface treatment on the tribological behavior of 17-4PH steel produced via binder jetting. Lubricants 13:42. https://doi.org/10.3390/lubricants13020042
15. Kalami H, Urbanic J (2021) Exploration of surface roughness measurement solutions for additive manufactured components built by multi-axis tool paths. Addit Manuf 38(December 2020):101822. https://doi.org/10.1016/j.addma.2020.101822
16. Cabanettes F et al (2018) Topography of as built surfaces generated in metal additive manufacturing: A multi scale analysis from form to roughness. Precis Eng 52(December 2017):249–265. https://doi.org/10.1016/j.precisioneng.2018.01.002
17. Radziejewska J, Marczak M, Maj P, Głowacki D (2023) The influence of vibro-assisted abrasive processing on the surface roughness and sub-surface microstructure of inconel 939 specimen made by LPBF. Materials 16(23). https://doi.org/10.3390/ma16237429
18. Liu W, Wang S, Jiang Q, Morgan M, Liu X (2022) Study on the motion characteristics of abrasive media in vibratory finishing. J

Phys Conf Ser 2198(1). https://doi.org/10.1088/1742-6596/2198/1/012035
19. Gillespie LK, LaRoux K (2007) Mass finishing handbook. Industrial Press
20. Yuvaraj HK, Gopasetty SK, Nagalingam AP, Sheng BGR, Gopinath A, Yeo SSH (2024) Effect of in-trough and out-of-trough fixturing in vibro-polishing. Proc Inst Mech Eng Part B J Eng Manuf 238(5):707–720. https://doi.org/10.1177/09544054231179246
21. Bańkowski D, Spadło S (2017) Vibratory Machining Effect on the Properties of the Aaluminum Alloys Surface. Arch Foundry Eng 17(4):19–24. https://doi.org/10.1515/afe-2017-0124
22. Eifler M, Garretson IC, Linke BS, Das J, Torner F, Seewig J (2019) Effects of vibratory finishing of 304 stainless steel samples on areal roughness parameters: A correlational analysis for anisotropy parameters. J Mater Process Technol 273:116256. https://doi.org/10.1016/j.jmatprotec.2019.116256
23. Damian B, Daniel K, Piotr M (2017) Deburring and Smoothing the Edges Using Vibro-abrasive Machining. Procedia Eng 192:28–33. https://doi.org/10.1016/j.proeng.2017.06.005
24. Pozzi M, Leone M, Sala L, Gottschalk A, Lucchini A, Huspek, Franz S (2025) Innovative mass finishing processes for intrinsically porous stainless steel components produced by metal injection moulding. Int J Adv Manuf Technol 140(1):951–968. https://doi.org/10.1007/s00170-025-16200-8
25. Stańczyk M, Figlus T (2019) The effect of selected parameters of vibro-abrasive processing on the surface quality of products made of 6082 aluminium alloy. Mater (Basel) 12(24). https://doi.org/10.3390/ma12244117
26. Bańkowski D, Spadło S (2019) The influence of abrasive paste on the effects of vibratory machining of brass. Arch Foundry Eng 19(3):5–10. https://doi.org/10.24425/afe.2019.129622
27. Boschetto A, Bottini L, Macera L, Veniali F (2020) Post-processing of complex SLM parts by barrel finishing. Appl Sci 10(4). https://doi.org/10.3390/app10041382
28. Nalli F, Bottini L, Boschetto A, Cortese L, Veniali F (2020) Effect of industrial heat treatment and barrel finishing on the mechanical performance of Ti6Al4V processed by selective laser melting. Appl Sci 10(7). https://doi.org/10.3390/app10072280
29. Sorocki J et al (2024) Low-Cost Method for Internal Surface Roughness Reduction of Additively Manufactured. IEEE Trans Microw Theory Tech 72(8):4519–4529. https://doi.org/10.1109/TMTT.2024.3361976
30. Bagehorn S, Wehr J, Maier HJ (2017) Application of mechanical surface finishing processes for roughness reduction and fatigue improvement of additively manufactured Ti-6Al-4V parts. Int J Fatigue 102:135–142. https://doi.org/10.1016/j.ijfatigue.2017.05.008
31. Atzeni E et al (2020) Performance assessment of a vibro-finishing technology for additively manufactured components. Procedia CIRP 88:427–432. https://doi.org/10.1016/j.procir.2020.05.074
32. Jamal M, Morgan MN (2017) Design process control for improved surface finish of metal additive manufactured parts of complex build geometry. Inventions 2:1–18. https://doi.org/10.3390/inventions2040036
33. Candela V et al (2022) Smoothening of the down-skin regions of copper components produced via Laser Powder Bed Fusion technology. Int J Adv Manuf Technol 123(9–10):3205–3221. https://doi.org/10.1007/s00170-022-10408-8
34. Rifat M, Demeter E, Basu S (2024) Evolution of Surface Roughness of Wrought and Additively Manufactured Inconel 718 During Centrifugal Disc Finishing. J Min Met Mater Soc 76:2835–2848
35. Fan F, Jalui S, Manogharan G (2023) Mass finishing of additively manufactured Ti6Al4V parts: An investigation of surface finish dependency on build orientation and processing conditions. Manuf Lett 35:439–449. https://doi.org/10.1016/j.mfglet.2023.08.095
36. Mofazali P, Dustmohamadi Z, Atapour M et al (2025) Tailoring surface characteristics of laser powder bed fusioned AISI 316L stainless steel for biomedical applications. Prog Addit Manuf 10:5009–5024. https://doi.org/10.1007/s40964-024-00882-9
37. Hähnel H et al (2024) Surface finishing of additive manufacturing parts for particle accelerators. Proc - Linear Accel Conf LINAC 367–370. https://doi.org/10.18429/JACoW-LINAC2024-TUPB020
38. Soja A, Li J, Tredinnick S, Woodfield T (2021) Surface finishing of additively manufactured stainless steel surgical instruments. Rapid Prototyp J 27(1):59–70. https://doi.org/10.1108/RPJ-01-2020-0009
39. Wang Y, Hu D (2005) Study on the inner surface finishing of tubing by magnetic abrasive finishing. Int J Mach Tools Manuf 45(1):43–49. https://doi.org/10.1016/j.ijmachtools.2004.06.014
40. Grizzle AC, Elliott A, Klein KL, Tyagi P (2024) Surface finishing and coating parameters impact on additively manufactured binder-jetted steel–bronze composites. Materials 17:598. https://doi.org/10.3390/ma17030598
41. Lecis N et al (2021) Effects of process parameters, debinding and sintering on the microstructure of 316L stainless steel produced by binder jetting. Mater Sci Eng A 828:142108. https://doi.org/10.1016/j.msea.2021.142108
42. Lores A, Naiara A, Iñigo A, and E. and, Zuza (2019) A review on recent developments in binder jetting metal additive manufacturing: materials and process characteristics. Powder Metall 62(5):267–296. https://doi.org/10.1080/00325899.2019.1669299
43. ASTM International (2019) Standard specification for hot-rolled and cold-finished age-hardening stainless steel bars and shapes (ASTM A564/A564M-19a). ASTM International, West Conshohocken
44. Huber D, Vogel L, Fischer A (2021) The effects of sintering temperature and hold time on densification, mechanical properties and microstructural characteristics of binder jet 3D printed 17–4 PH stainless steel. Addit Manuf 46:102114
45. Radhakrishnan J, Kumar P, Gan SS, Bryl A, McKinnell J (2022) Ramamurty. Microstructure and tensile properties of binder jet printed 17–4 precipitation hardened martensitic stainless steel. Mater Sci Eng A 860:144270
46. Cho Y-H, Park S-Y, Kim J-Y (2023) Lee. 17-4PH stainless steel with excellent strength–elongation combination developed via material extrusion additive manufacturing. J Mater Res Technol 24:3284–3299. https://doi.org/10.1016/j.jmrt.2023.03.228
47. ISO (2018) ISO 10993-1:2018 Biological evaluation of medical devices—Part 1: Evaluation and testing within a risk management process. International Organization for Standardization, Geneva
48. Afonso Camargo SE et al (2020) Anti-bacterial properties and biocompatibility of novel SiC coating for dental ceramic. J Funct Biomater 11(2). https://doi.org/10.3390/jfb11020033

Authors and Affiliations

Matteo Pozzi[1,2] · Andrea Lucchini Huspek[1] · Marco Mariani[3] · Sara Candidori[3] · Serena Graziosi[3] · Nora Lecis[3] · Silvia Franz[1] · Massimiliano Bestetti[1]

✉ Matteo Pozzi
matteo.pozzi@polimi.it

Andrea Lucchini Huspek
andrea.lucchinihuspek@polimi.it

Marco Mariani
marco.mariani@polimi.it

Sara Candidori
sara.candidori@polimi.it

Serena Graziosi
serena.graziosi@polimi.it

Nora Lecis
nora.lecis@polimi.it

Silvia Franz
silvia.franz@polimi.it

Massimiliano Bestetti
massimiliano.bestetti@polimi.it

[1] Department of Chemistry, Materials and Chemical Engineering "Giulio Natta", Politecnico di Milano, Via Bassini 6, Milano 20133, Italy

[2] Rösler Italiana S.r.l, via Elio Vittorini 10/12, Concorezzo (MB) 20863, Italy

[3] Department of Mechanical Engineering, Politecnico di Milano, via privata Giuseppe La Masa 1, Milano 20156, Italy